



Numerical analysis of shipping water impacting a step structure

Danial Khojasteh^a, Sasan Tavakoli^b, Abbas Dashtimanesh^c, Azam Dolatshah^{b,d},
Luofeng Huang^e, William Glamore^a, Mahmood Sadat-Noori^a, Gregorio Iglesias^{f,g,*}

^a Water Research Laboratory, School of Civil and Environmental Engineering, UNSW Sydney, NSW, Australia

^b Department of Infrastructure Engineering, University of Melbourne, Parkville, 3031, VIC, Australia

^c Estonian Maritime Academy, Tallinn University of Technology, Kopli, 11712, Tallinn, Estonia

^d Faculty of Science, Engineering and Technology, Swinburne University of Technology, Hawthorn, 3122, VIC, Australia

^e Department of Mechanical Engineering, University College London, London, UK

^f MaREI Centre, Environmental Research Institute & School of Engineering, University College Cork, College Rd., Cork, Ireland

^g School of Engineering, University of Plymouth, Marine Building, Drake Circus, Plymouth, PL4 8AA, UK

ARTICLE INFO

Keywords:

Green water
Floating structures
Dam-break
Impact force
CFD
OpenFoam

ABSTRACT

Shipping water, the flow washing over and impacting the upper decks of ships and offshore structures, occurs frequently during their service life and often causes structural problems. For engineers to design safe floating structures subjected to shipping water it is essential to gain an in-depth understanding of its depth and flow field, and the resulting impact forces. In this work, Computational Fluid Dynamics (CFD) is applied to understand the physics of shipping water washing over a stepped platform. We find that the most accurate solutions are obtained with the $k - \epsilon$ turbulence closure. The hydrodynamic load generated by the shipping water is found to strongly depend on the kinematic energy of the water hitting the step. It is shown that with smaller values of the freeboard a more dynamic flow ensues, with a stronger vortex and larger velocity gradient resulting in deeper shipping water and a larger impact force.

1. Introduction

Shipping water, also known as green water, is the water flow washing the upper deck of ships and offshore structures, which can exert large forces (responsible for 10% of sea loads, see Hirdaris et al., 2014) and result in motions (Dillingham, 1981; Greco et al., 2015), deformations (Buchner, 1995), and the loss of transverse stability as the centre of gravity can be shifted upwards (Ersdal and Kvitrud, 2000). These problems have a complicated nature and can be caused by different mechanisms, e.g., waves and hurricanes (O'Dea et al., 1992; Mori and Cox, 2003; Faltinsen et al., 2005). In the last decades, intensive efforts have been devoted to modelling this problem, using various physical, analytical and numerical models. It is essential to understand the impact loads, their physics, and the kinematic of the flow washing the body, amongst other issues, to provide safer operating conditions for ships or offshore structures (, 2005; Fonesca and Soares; Faltinsen et al., 2004).

Shipping water occurs when water overtops the freeboard of the

floating object (Faltinsen et al., 2002), and is induced by any perturbation, typically water waves (Longuet Higgins and Cokelet, 1976; Cox and Scott, 2001). The wave then collapses and runs on the upper surface of the floating object (Dolatshah et al., 2018), which can be either a ship or an offshore structure. Depending on the nature of the source (the mechanism of formation), the impact forces acting on the deck can be different, i.e., the water column collapsing can have different values of kinematic and potential energy, which may lead to different impact forces (Ariyaratne et al., 2012). One of the most common types of shipping water is via plunging waves, i.e., the wave crest exceeds the freeboard and then runs across the deck, eventually adopting a shallow water pattern (Greco et al., 2005). In this case, it is expected that the kinematic energy is the highest contributor to the external forces. Such phenomenon is probable when the freeboard of the floating object is small, so that gentle waves can propagate on the deck. It has been found that a very steep wave breaking in the vicinity of the deck can lead to an energetic plunging pattern, which then washes the upper surface of the deck (Greco and Colicchio, 2007). The plunging pattern that appears

* Corresponding author. MaREI Centre, Environmental Research Institute & School of Engineering, University College Cork, College Rd., Cork, Ireland.

E-mail addresses: danial.khojasteh@unsw.edu.au (D. Khojasteh), stavakoli@student.unimelb.edu.au (S. Tavakoli), abbas.dashtimanesh@taltech.ee (A. Dashtimanesh), adolatshah@swin.edu.au (A. Dolatshah), luofeng.huang.15@ucl.ac.uk (L. Huang), w.glamore@wrl.unsw.edu.au (W. Glamore), m.sadat-noori@unsw.edu.au (M. Sadat-Noori), gregorio.iglesias@ucc.ie (G. Iglesias).

<https://doi.org/10.1016/j.oceaneng.2020.107517>

Received 21 February 2020; Received in revised form 5 May 2020; Accepted 9 May 2020

Available online 5 June 2020

0029-8018/© 2020 The Author(s). Published by Elsevier Ltd. This is an open access article under the CC BY license (<http://creativecommons.org/licenses/by/4.0/>).

after the breaking can run across the water surface (following a highly nonlinear pattern) and then wash the surface of the deck, resulting in large forces (Chan and Melville, 1988; Cuomo et al., 2010). A combination of kinematic energy and potential energy contributes to the generation of an impact force. This pattern is seen to occur when the water column exceeds the deck height (Buchner, 2002). Such a mechanism is more probable when motions of the vessel or floating object are large (Ogawa et al., 2002). A dam-break behaviour has also been described as another type of shipping water, for which analytical solutions exist, as will be explained later.

The modelling of the shipping problem can be performed using mathematical methods (Greco et al., 2004), with certain assumptions, including the neglect of the viscosity and vorticity. One of the most common methods implemented to simulate the waters running on the upper surface of a floating object is to use the dam-breaking solution (Schonberg and Rainey, 2002; Ryu et al., 2007). The dam-break problem can be solved analytically (e.g., Yilmaz et al., 2013), and hence, the details of the flow field (Chuang et al., 2015) or the loads (Greco et al., 2001) can be obtained. These theoretical solutions are helpful in the early understanding of the physics of the problem (Stansby et al., 1998; Yilmaz et al., 2003). However, many aspects of the problem are disregarded such as energy dissipation, wave breaking, motion coupling, etc.

To overcome these limitations, a shallow-wave numerical modelling approach has been used (Huang and Hsiung, 1996; Greco and Lungu 2012a,b; Skene et al., 2018). In this approach, single-phase flow is assumed, i.e., no air flow is considered, implying that breaking processes cannot be modelled. For this reason, the energy of the shipping water is likely to be overpredicted (Hernández-Fontes et al., 2019b) and so are the loads if breaking of running water occurs.

As an alternative, Computational Fluid Dynamics (CFD) can be used to simulate the washing of shipping water over any floating object (Stern et al., 2001). This method has shown significant potential in modelling sea loads (Izadi et al., 2018a), dynamic responses (Zhou et al., 2019; Esfandiari et al., 2019), resistance (Tezdogan et al., 2015; Kim et al., 2017; Demirel et al., 2017; Khojasteh and Kamali, 2017; Ghadimi et al., 2019; Huang et al., 2019b, 2020; Nazmand Bilandi et al., 2020; Dash-timanesh et al., 2020) and wave energy (Bayoumi et al., 2015; Khojasteh and Kamali, 2016; Khojasteh et al., 2018a; Khojasteh et al., 2018b; Lopez et al., 2014; Masida et al., 2019) in the last three decades, and its application has become ever more common in recent years (Larsson et al., 2013).

Different computational methods, including Finite Volume Method (FVM) and Smoothed Particle Hydrodynamics (SPH), can adequately simulate two-phase flow (Stern et al., 2006). Among these methods, SPH has been found to accurately model the free water surface, while it can under-predict the pressure of the fluid field (Landrini et al., 2012; Dashtimanesh and Ghadimi, 2013; Ghadimi et al., 2012). The FVM, which uses different numerical techniques, has been shown to effectively predict both sea loads and water surfaces (Ghadimi et al., 2013). CFD methods can be successfully applied to capture different properties of the fluid, including shear stresses, energy flux, and mass flux (Khojasteh et al., 2017; Javanmardi et al., 2018), while they can also be coupled with solid mechanic solvers (Izadi et al., 2018b; Huang and Thomas, 2019; Huang et al., 2019a). With recent advances in high-performance computing, CFD methods have taken a valuable position in the early stage design of ships and offshore structures (Xie et al., 2019).

In recent years, CFD studies have been undertaken to model the green water running on the upper surface of ships/offshore structures with good accuracy (Nielsen and Mayer, 2004; Silva et al., 2017; Amaro Jr et al., 2019; Zhang et al., 2019; Chen et al., 2019; Gatin et al., 2018a, 2019). However, there is still an opportunity for CFD studies of shipping water since the behaviour of the flow, including the velocity field and the energy flux is not fully understood. One of the most important aspects of the shipping water relates to the energy of the water, and its

relationship with force and other physical aspect of the problem. Such phenomenon can be studied through modelling of isolated waves that can be generated using the dam-breaking near step. In the recent years, experiments have been performed, reporting on the behaviour of the fluid field when water, caused by dam-breaking, is transported across the upper surface of the deck.

In the current paper, CFD simulations are used to improve the understanding of the physics of the dam-break water washing on a stepped platform. First, the accuracy of the CFD method is shown to be fit for purpose (i.e., it is shown that it can compute the fluid field accurately). Then, detailed results are presented to deepen the understanding of the fundamental physics (velocity field, velocity gradient, energy flux, impact force and how they are linked to each other) of shipping water caused by a dam-break. In all, this study seeks to compute the energy of the fluid, the forces acting on the stepped platform, and the velocity profile of the fluid in different conditions.

The paper is organized as follows: In Section 2, the numerical model is discussed by explaining the problem, case study, governing equations, and the CFD set-up. In Section 3, the obtained results are provided; initially focusing on the optimal grid size for the problem simulation. A validation study is performed and the CFD data are compared against the experimental data. Finally, the changes in flow field are discussed in detail. In Section 4, the concluding remarks and potential future research are presented.

2. Numerical model

2.1. Problem statement

The breaking of a dam is simulated in the current problem to numerically replicate the experimental work performed by Hernández et al. (2018) and Hernández-Fontes et al. (2018), and further elucidate the underlying physics. A 0.195 m long step with a height of h_s is located in the right end of a tank. A virtual gate, located at a longitudinal location of l_g with respect to the left end of the tank, is assumed to be in the tank, and keeps the water column in a steady condition. This gate is suddenly removed, triggering a dam break, which can then run onto the stepped platform. Such phenomenon resembles the shipping water on the deck of a fixed floating structure subjected to solitary waves and helps to understand the behaviour of green water in absence of reflection effects. The tank is three-dimensional and is b_T wide. The depth of the water located in the left side of the gate is shown by h_d (dam height) and the water depth on the right side is denoted with h_w (water height). A sketch of the tank is shown in Fig. 1. The freeboard of the step, is computed as:

$$h_{FB} = h_s - h_w \quad (1)$$

2.2. Governing equations

The fluid is assumed to be viscous and two phases are considered, water and air. The relationship between viscosity and shear stresses in a Newtonian fluid governs the flow. Both phases behave as an incompressible fluid. The fluid field is denoted by $\mathbf{u} = u_x\mathbf{i} + u_y\mathbf{j} + u_z\mathbf{k}$. The Navier-Stokes equations hold in the entire domain:

$$\nabla \cdot \mathbf{u} = 0, \quad (2)$$

$$\partial_t(\rho_e \mathbf{u}) + \nabla \cdot (\rho_e \mathbf{u}) \mathbf{u}^T = -\nabla p + \nabla \cdot (\mu_e + \mu_t) [\nabla \mathbf{u} + (\nabla \mathbf{u})^T] + \rho_e \mathbf{f}_b, \quad (3)$$

where the subscript e refers to the effective value of the parameter; ρ and μ refer to the density and viscosity of the fluid, respectively; p is the pressure and $\mathbf{f}_b = -g\mathbf{k}$, is the body force. Note that μ_t refers to the turbulence viscosity and is found using the $k-\varepsilon$ model. The effective values of density and viscosity are computed by means of a volume fraction parameter, which is set to vary between 0 and 1 (Hirt and

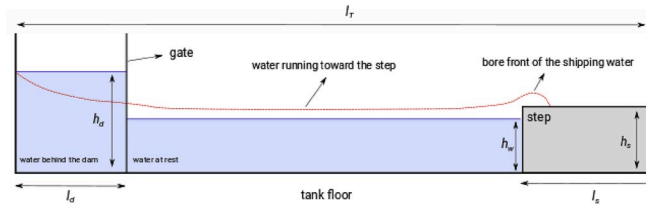


Fig. 1. Schematic of shipping water caused by a dam-break. The filled area shows the water level before the gate is released. The thick line shows the gate. The dashed red line is the water surface as water reaches the step. (For interpretation of the references to colour in this figure legend, the reader is referred to the Web version of this article.)

Nichols, 1981). Whenever the parameter takes a value of 0 it denotes the pure air, whereas value of 1 denotes the pure water. Using the value of α , Equations (4) and (5) are used to find effective values of density and viscosity, respectively.

$$\rho_e = \alpha\rho_w + (1 - \alpha)\rho_a \quad (4)$$

$$\mu_e = \alpha\mu_w + (1 - \alpha)\mu_a \quad (5)$$

The parameter α obeys a conservation law itself, which can be formulated as:

$$\partial_t \alpha + \nabla \cdot (\alpha \mathbf{u}) + \nabla \cdot [\mathbf{u}_r \alpha (1 - \alpha)] = 0, \quad (6)$$

where \mathbf{u}_r is the surface compression velocity.

2.3. Numerical set-up

The problem is numerically solved using a CFD code, based on FVM. The numerical set-up and simulations are performed using the OpenFoam library, which has shown promising ability to model free surface flows (e. g. in Higuara et al., 2013; 2014a, b; Gatin et al., 2018b). To perform the simulations, the tank is numerically generated using the BlockMeshDict. The schematic of the tank is shown in Fig. 2. The walls of the tank, both right and left sides, satisfy a no-slip condition. This means that both the zero-gradient speed and pressure conditions are governed there. The same condition is also set on the walls of the step. The upper patch of the domain is set to behave as an area from which fluid can leave the domain. The velocity in the whole domain is initially set to zero. The value of the volume fraction is set to 1 at the left and right side of the virtual gate. For the rest of the domain, α is set to 0. The cells in the domain are produced using a structured grid with a rectangular cube shape. The cells have a smaller size near the step and at the free water surface, with larger mesh sizes with distance from the domain of interest. The numerical mesh is shown in Fig. 2.

All diffusion terms are discretised using a second-order central scheme and the convection terms are turned into algebra equations using a linear approximation. The unsteady terms are discretised in the time domain by means of a Euler Scheme. The simulations are

performed for more than a second after the dam-break occurs (like the experiments). The time step is set to be adjusted automatically by forcing the Courant number to be less than 0.5. The Navier-Stokes equations are solved using the PISO (Pressure-Implicit with Splitting of Operators) algorithm, and the InterFoam solver (Jasak, 2009; Vukcevic et al., 2018).

2.4. Computation of different parameters

The water surface elevation at any point is found using a virtual probe. To serve this purpose, the OpenFoam library is used to sample all data at different plans. The values of α , \mathbf{u} and p are extracted at all-time steps. All data are sampled at a frequency of 50 Hz. The instantaneous elevation of the free surface is computed as:

$$\eta(x, z) = \int_{z_f \text{ or } z_s}^{z_u} \alpha(x, z) dy \quad (7)$$

Note that z_u refers to the vertical position of the upper boundary of the domain. z_f and z_s denote the vertical position of the lower boundary (tank floor) and the step, respectively. The vorticity is calculated by:

$$\omega(x, y, z) = \frac{1}{2} \nabla \times \mathbf{u}(x, y, z) \quad (8)$$

The force acting on the step is calculated by integrating the pressure and stresses on the surface of the step as follows:

$$F = \int_S (p \mathbf{n} + \boldsymbol{\sigma} \cdot \mathbf{n}) dS \quad (9)$$

where $\boldsymbol{\sigma}$ denotes the stresses and \mathbf{n} is the unit normal vector.

The energy flux, related to kinetic energy and potential energy, passing through the water column (Whitham, 1962) is measured as:

$$\dot{E} = \int_{z_f \text{ of } z_s}^{z_u} \left(\frac{1}{2} |\mathbf{u}|^2 + gz \right) \rho_w \alpha u_n dz \quad (10)$$

2.5. Case studies

Seven cases were modelled numerically (Table 1), corresponding to the laboratory tests conducted by Hernández-Fontes et al. (2018, 2019a). In each case, different values of h_d and h_w are used. Note that the ratios of h_d/h_w are set to be 0.4 and 0.6 during the tests, which satisfy the bore generation condition during the dam-breaking (Nakagawa et al.,

Table 1

Case studies considered in the present study.

Case No.	h_d	h_w	h_d/h_w	h_{FB}
1	0.108	0.180	0.6	0.042
2	0.120	0.200	0.6	0.030
3	0.126	0.210	0.6	0.024
4	0.132	0.220	0.6	0.018
5	0.144	0.240	0.6	0.006
6	0.108	0.270	0.4	0.042
7	0.120	0.300	0.4	0.030

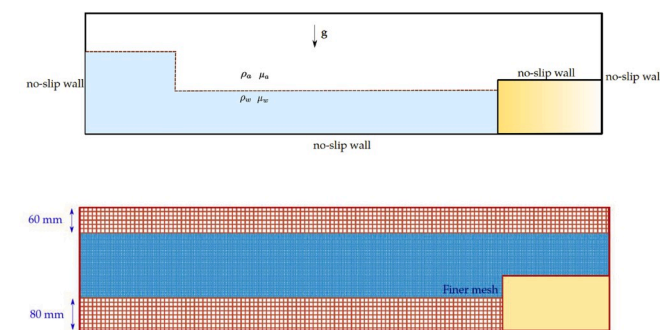


Fig. 2. Computational domain (up) and computational grid (down). A structured grid is used and the spacing near the tank floor and upper surface of the tank are set to be larger.

Table 2

Features of the tanks used for simulation of the shipping water (details can be found in Hernández-Fontes et al. (2018, 2019a).

Tank No.	l_s	L_T	l_d (mm)	b_T (mm)	h_s (mm)	h_T (mm)
1	195	1000	300	335	150	450
2	392	1950	300	500	150	450

1969). The details of the numerical tests are given in Table 2. Technical information related to the experiments is reported in Hernández-Fontes et al. (2017). The length of the tank varies because two different tanks were used by Hernández-Fontes et al. (2018, 2019a).

3. Results and discussion

3.1. Grid convergence study

A grid study was performed to determine the optimal numerical mesh resolution for the simulations. To this end, different grids, including coarse, medium, fine and finest are used. The coarse grid mesh contains cells with a dimension of $5 \times 5 \times 5\text{mm}^3$ around the step, and the finest grid contains cells with dimension of $0.5 \times 0.5 \times 0.5\text{mm}^3$ in the proximity of the step. Details of different grids tested are presented in Table 3. Simulations are performed for all cases using different mesh resolutions. Throughout the mesh study, it has been found that the results, including water surface elevation, time energy flux, forces acting on the step, and the vorticity field converged for the fine mesh resolution. The mesh study results are summarised in Fig. 3.

The maximum values for the water surface elevation and maximum depth of the shipping water are indicated in Fig. 3. This simulated depth versus the modelled depth was shown to converge for a mesh size of $1 \times 1 \times 1\text{mm}^3$. Also, the vorticity field around the step is found to converge for a mesh size of $1 \times 1 \times 1\text{mm}^3$ (fine mesh). The results found using the fine and finest mesh are similar.

Note that the water surface elevation is computed at a point with a non-dimensional longitudinal distance of $0.0130L_s$ (L_s is the length of step) from the front edge of step. The computed vorticity fields around the body were also found, demonstrating that the vorticity fields using the fine and finest mesh are in good agreement as illustrated in Fig. 4. However, the vorticity fields computed using the medium and coarse mesh resolution are different. For the case of coarse and medium grids, the water surface is not smooth and larger energy dissipation occurs near

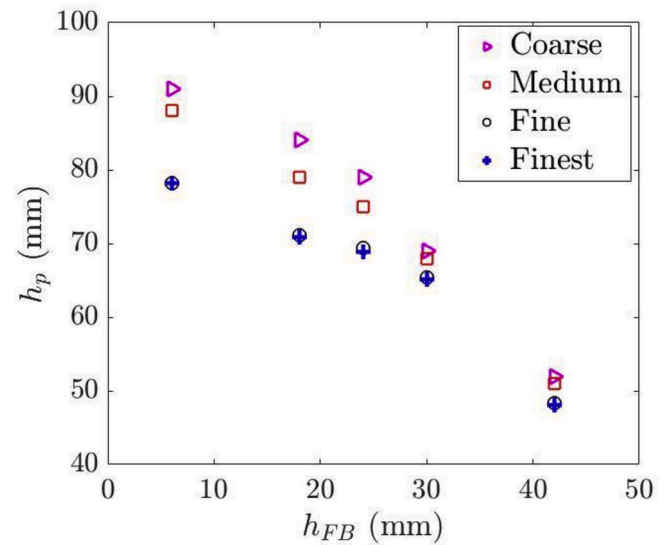


Fig. 3. Mesh convergence study showing maximum water surface elevation (h_p) versus freeboard (h_{FB}) for the shipping water at a distance of $0.0130L$ from the front edge of the step. (Dam-break in Tank 1).

Table 3

Details of the computational grids tested in this study.

Grid type	Mesh size (mm^3)
Coarse	$5 \times 5 \times 5$
Medium	$2.5 \times 2.5 \times 2.5$
Fine	$1 \times 1 \times 1$
Finest	$0.5 \times 0.5 \times 0.5$

Table 4

Water surface elevation maxima and corresponding errors between numerical and experimental results for different simulation cases in Tank 1. The recorded values correspond to the point with a longitudinal position of $0.0130L_s$ from the step edge. Experimental data is taken from the work published by Hernández-Fontes et al. (2018).

Case No.	h_{p-t} (mm)	h_{p-l} (mm)	h_{p-exp} (mm)	e_t	e_l
1	48.34	52.96	47.65	1.45	11.14
2	65.35	67.11	61.95	5.49	8.33
3	69.37	72.83	66.10	4.95	10.18
4	71.19	73.41	67.95	4.77	8.04
5	78.22	81.16	74.00	5.70	9.68
6	104.97	108.32	99.85	5.13	8.48
7	124.41	129.83	118.30	5.16	9.75

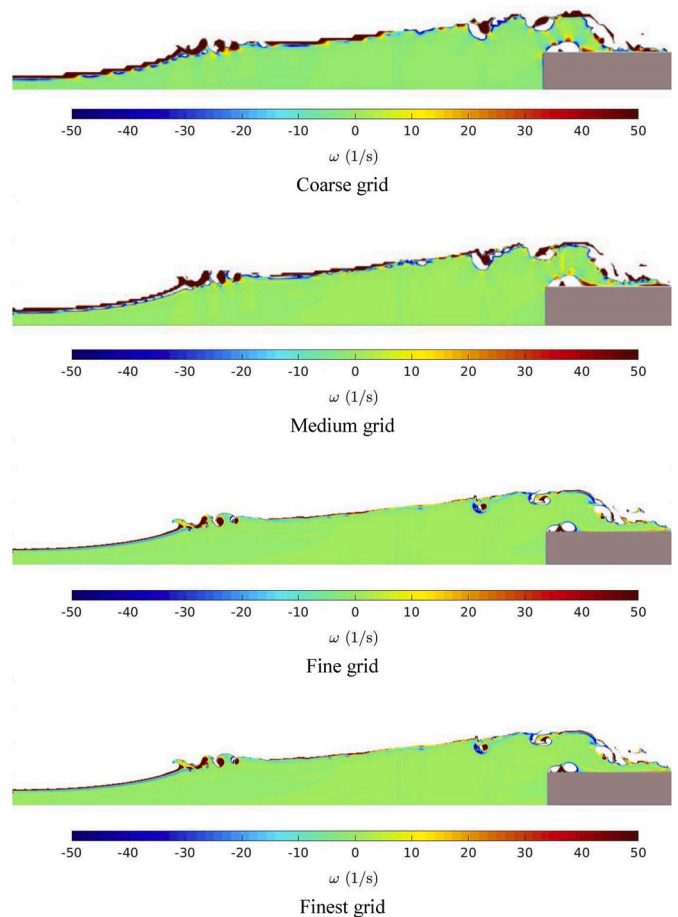


Fig. 4. Vorticity (ω) for Case 4 with different grid sizes. (Dam-break in Tank 1).

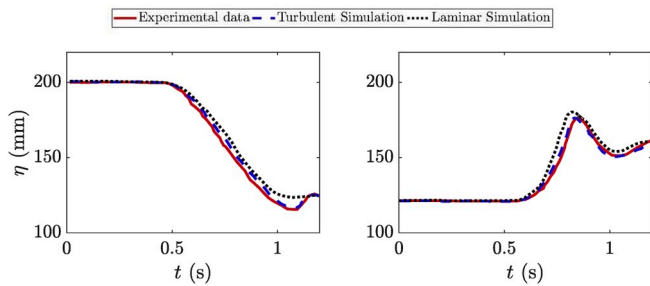


Fig. 5. Time evolution of the water surface elevation in front of the step at two longitudinal positions: $x = 0.15$ m (left panel), and $x = 0.45$ m (right panel). Both panels correspond to Case 2 in Tank 1.

the free surface (the red colour). Therefore, the fine mesh is used for all the simulation cases in the present study.

3.2. Experimental data versus CFD data

Here, the obtained CFD data are compared against the experimental measurements of Hernández-Fontes et al. (2018, 2019a) to check the accuracy of the numerical platform. Both the laminar and the turbulent simulations are employed to evaluate the accuracy of both methods. Three groups of comparisons are performed. At the first step, the water surface elevation in the left side of the step (not on the step) is computed, and its value is compared against laboratory measurements of Hernández-Fontes et al. (2018). Subsequently, the water surface elevation on the stepped platform is found and quantitatively compared against experiments of Hernández-Fontes et al. (2019a) and Hernández-Fontes et al. (2018). In the last step, the computed impact force is qualitatively compared against measurements of Hernández-Fontes et al. (2019a, 2019b).

3.2.1. Water surface level in the front field: left side of the step

Water surface elevations at two different locations in the front field, the field at which the dam-breaking occurs, are computed. Two (virtual) probes are assumed and the water height is found using Equation (7). These probes were located at the centreline of the tank at longitudinal positions of 0.15 and 0.45 m, with respect to the left wall of the tank.

Simulations were performed for Case 2 (see Table 1). The values of the free surface elevation at these two points have been reported by

Hernández-Fontes et al. (2018). The time histories of water surface elevation at $x = 0.15$ m (left panel) and $x = 0.45$ m (right panel) are shown in Fig. 5. Two different numerical simulations, laminar and turbulent flows are used. The water surface elevation is observed to decrease on the left side of the gate as expected (since it is breaking) and then slightly increase again (left panel). Both CFD models are found to follow the experimental results, but the laminar simulation is observed to marginally over-predict the water level. There is also a hallow (between $t = 1$ to $t = 1.2$ s) in the plot which was not detected by the laminar simulation. This behaviour of the water surface on the left side of the dam is observed by different researchers (e. g. Kleefsman et al., 2005). The water surface increases and reaches a peak value on the right side of the gate. Note that the dam break phenomenon occurs, and water is running toward the right side of the gate (Zech and Soares-Fraza, 2007). As the water level reaches a peak, its value decreases and then it starts to increase around $t = 1$ s, i.e., a slight harmonic behaviour, which is being dampened. Further, the water surface tends to reach an equilibrium (Hui et al., 2017). The turbulent simulation presents more accurate results as the real nature of the flow (turbulence) is captured (Na et al., 2016). The laminar simulation results in larger water surface and the peak is predicted to occur sooner as found by Taha et al. (2018). This difference occurs as the turbulent behaviour is neglected and less energy dissipation is predicted.

3.2.2. Water surface level on the step

Computed water depth on the stepped platform were compared against experimental data. Water height at four different points with longitudinal locations of $x/L_s = 0.0388, 0.0898, 0.1408$ and 0.1918 are reported below with laminar and turbulent simulations performed for all cases. The results corresponding to Case 1 are shown in Fig. 6. The water surface elevation is seen to reach a peak value and then decrease and converge to zero. The further the location from the wave break results in a smaller peak value. Note that this peak value is experimentally observed when waves wash the deck of a floating object (Greco et al., 2012b). In the current research, the shipping wave is generated using a dam-break flow approach and hence, only one peak is evident.

Both CFD simulations predict the time-history of water surface elevation as per the experimental data, but the turbulent simulation is found to be more accurate, especially for the points near the edge of the step. The laminar simulations lead to over-prediction of the water surface elevation, due to the smaller amount of energy dissipation computed under the laminar assumptions (Gush et al., 2007).

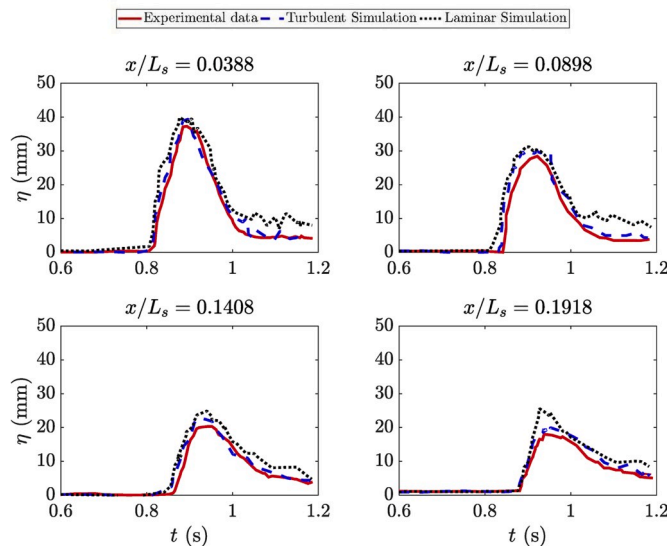


Fig. 6. Time histories of the water surface elevation at different points on the step. (Case 1, Tank 2).

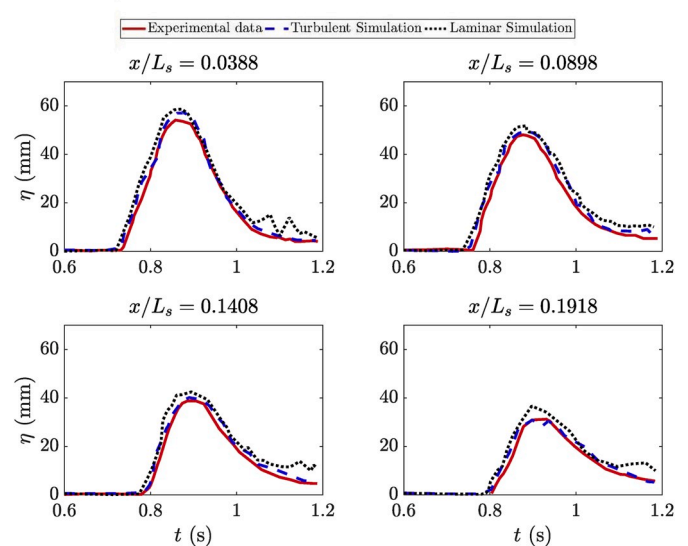


Fig. 7. Time histories of the water surface elevation at different points on the step. (Case 3, Tank 2).

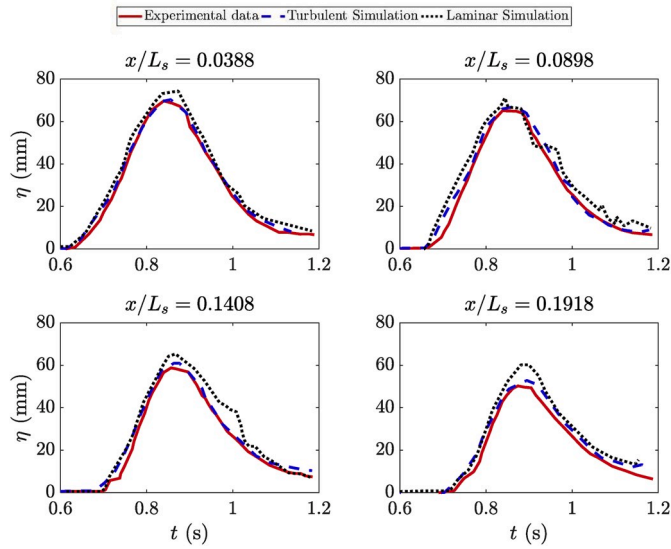


Fig. 8. Time histories of the water surface elevation at different points on the step. (Case 5, Tank 2).

Computed values of water surface elevation corresponding to Case 3 and Tank 2 are presented in Fig. 7. Experimental and numerical simulations are plotted. CFD results are more accurate for the turbulent simulation (as seen in Fig. 6). The tail of the water surface elevation vs. time plot is seen to fluctuate when the laminar flow simulation is used. The water surface, again, is higher, especially at the tail when turbulence behaviour of the fluid is neglected. The results corresponding to Case 5 and Tank 2 are also illustrated in Fig. 8. Note that water reaches a higher peak in this case (as compared to the two previous cases) and corresponding freeboard is lower. CFD data is shown to agree well with the experimental data, *i.e.*, numerically computed water surface is rising at the time the experimentally measured water surfaces rise. The time at which the peaks of water surface elevation occurs are found to be similar. Laminar simulations may over-predict the water surface level as was reported in Figs. 6 and 7.

The CFD results are also compared against the measurements performed in Tank 1. The maximum value of the water level (the wave crest) at a distance of $0.0130L_s$ from the edge of the step is found and compared against experiments. Note that Hernández-Fontes et al. (2018) reported the peak height of shipping water only for this point. Therefore, the quantitative comparisons are only performed for water depth at $0.0130L_s$. Table 3 shows the experimental and numerical results, as found using both laminar (shown by the l) and turbulent (subscript t) models. The computed values using the turbulent simulations are closer to the experimental data. Errors between numerical and experimental results are computed as per:

$$e = \frac{|h_{p-exp} - h_{p-num}|}{|h_{p-exp}|} \times 100 \quad (11)$$

where *exp* and *num* refer to experimental and numerical values, respectively. Errors are found to vary between 1.5 and 5.7 percent for the case of turbulent simulations, but they range between 8.3 and 11.1 percent for the case of laminar simulations.

3.2.3. Impact force acting on the step

The impact force (vertical force) acting on the step is computed for different cases in Tank 2. Note that the impact force was previously measured and reported by Hernández-Fontes et al. (2019b). An area with width of 334 mm ($0.852L$) and length of 195 mm ($0.4794L$) is considered to calculate the external forces as per Hernández-Fontes et al. (2019b). Time histories of the vertical force for three cases are

presented. The vertical force is seen to increase and reach a maximum value for all cases and then converge to zero. The largest impact force occurs for Case 5, where the step has the lowest freeboard. CFD results are shown to follow the experimental data for all cases. However, the turbulent simulations have less error compared to the laminar simulations. The force is seen to be over-predicted when simulations are performed for the case of a laminar fluid. Over-predictions are most significant at the peak and tail of the plots. Overall, the results show that current CFD model predicts the impact force accurately if turbulent flow is applied.

3.3. An overview of the flow washing the step

An example of the water washing over the step is depicted in Fig. 10. This corresponds to Case 3, with different snapshots over time at a 0.05s interval. The vorticity, computed by Equation (8), is also shown. Before the water reaches the step, a plunging wave caused by the dam-break moves towards the step, on which positive or negative vorticities occur due to energy dissipation as observed by De Padova et al. (2019). As the water reaches the step, the vorticities of the front edge of the bore become less significant, while considerable vorticities can be found further back. As the water impacts the step, a cavity occurs. As the bores move forward on the step, large vortices occur and energy dissipation becomes more significant (Skene et al., 2018). At the early stage of impact, the force acts on a very small area, but then the water column collapses and the force acts on the whole surface of the step, while the air cavity becomes smaller (Zhou et al., 1991). Examples of the vorticities found for Case 5 are also shown in Fig. 10, with similar behaviour observed at different time steps. As the bore moves toward the step, a small amount of vorticity exits on the front bore as it reaches the step. An air cavity is generated that directs the water flow forward. Water impacts a very small area at the beginning and then the area becomes larger while the vortices become significant near the surface of the step (see Fig. 11).

3.4. Physical understanding

In order to investigate the different physical mechanisms from each case, the numerical data is used to examine the behaviour of the energy, mass flux, pressure and cavity area. At an early stage, the energy fluxes of different cases have been calculated at the front edge of the step. Samples of the time history of the energy flux are shown in Fig. 12. Comparison between the energy fluxes of Cases 1 and 3 in Tank 2 are shown in the right panel. The energy fluxes are seen to increase at the early stage of shipping and then reach a peak. Following this peak, the flux of energy decreases and reaches negative values, meaning that energy is moving toward the tank again (mean velocity of the water flow is negative). Case 1 has seen to be less energetic compared to Case 3. Note that the step freeboard of the Case 3 is lower compared to Case 1. The smaller freeboard leads to more energetic flow on the surface of the step, resulting in a larger impact force (see Fig. 9) and free surface elevation (see Figs. 6 and 7). The right panel of Fig. 12 shows the comparison between energy fluxes at the edge of the step caused by Case 1 in Tanks 1

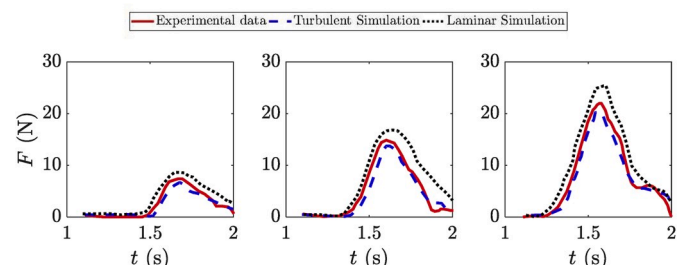


Fig. 9. Time histories of the impact force acting on the step.

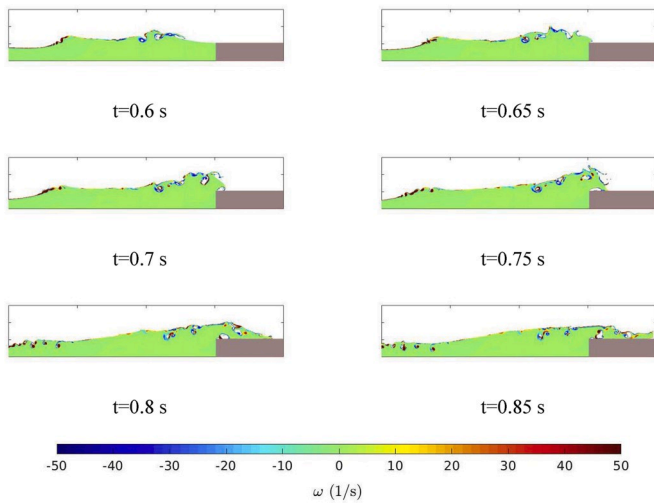


Fig. 10. Shipping water washing the deck of a step. Temporal snapshots present the vorticity field (ω) and correspond to Case 3 in Tank 1. The step is depicted by the grey box.

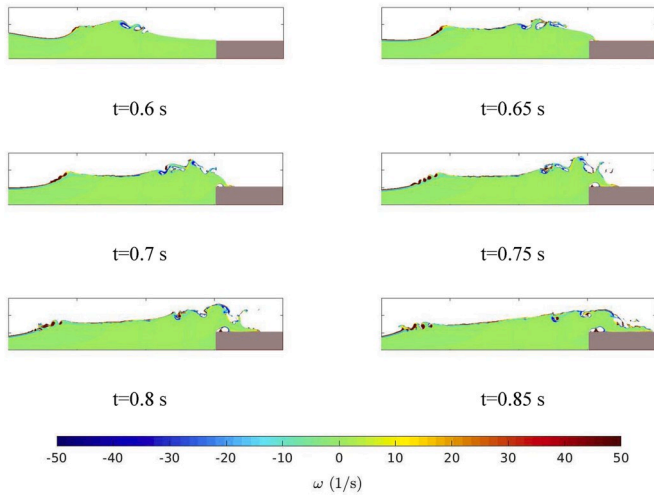


Fig. 11. Shipping water washing the deck of a step. Temporal snapshots present the vorticity field (ω) and correspond to Case 4 in Tank 1. The step is depicted by the grey box.

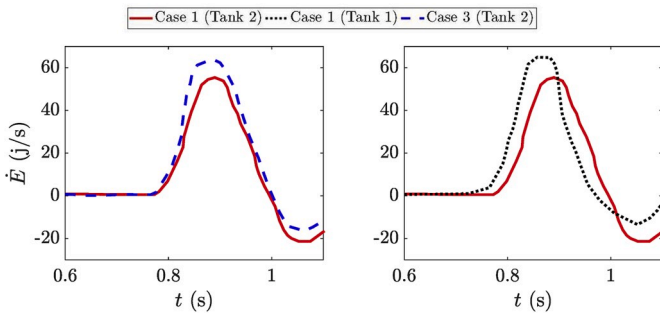


Fig. 12. Energy flux of the shipping water caused by the dam break washing the surface of a step. The left panel shows the comparison between the energy fluxes of Cases 1 and 3 (Tank 2). The right panel shows the energy fluxes of Case 1 in Tanks 1 and 2.

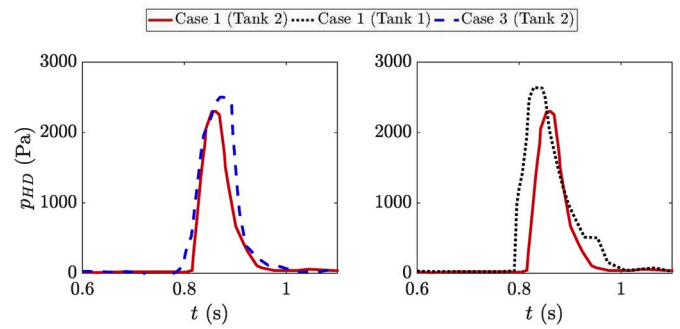


Fig. 13. Shipping water impact pressure caused by the dam break. The plot shows the time history of pressure at $x = 0.005$ m. Left panel shows comparison between energy fluxes of Cases 1 and 3 when dam-break occurs in Tank 2. Right panel shows the energy fluxes of Case 1 in Tanks 1 and 2.

and 2. Similar behaviour (to what was observed in the left panel) is noted. Energy fluxes reach a peak and then decrease, reaching negative values. The dam-break occurring in the Tank 1 is seen to lead to a more pronounced energy peak. Note that when water is running in the Tank 1, it travels a shorter distance to reach the step, thus it is more energetic (its kinematic energy is expected to be larger). This increased amount of energy is expected to lead to larger pressures and impact forces, as will be discussed later.

The time histories of the hydrodynamic pressure caused by the shipping water are evaluated. The hydrodynamic pressure is sampled at a point located at $x=0.005$ m from the step for different cases, and examples of the computations are shown in Fig. 13. The pressure increases sharply as the water reaches the surface, in line with previous research on wave impacts on structures (Jalalisenidi et al., 2018; Tavakoli and Dashtimanesh, 2019). After the sudden rise in hydrodynamic pressure, the pressure drops drastically, tending to zero. The pressures caused by the dam-break of Cases 1 and 3 in Tank 2 are displayed in the left panel of Fig. 13. Case 3 results in a larger impact pressure, which was expected given as the shipping flow of Case 3 is more energetic (left panel of Fig. 12). The impact pressure from Case 1 in the two Tanks of 1 and 2 is shown in the right panel of Fig. 13. When dam-break occurs in Tank 1, the peak pressure occurs earlier, and its value is more remarkable. This larger pressure occurs since water flow is more energetic in Tank 1 (as seen in the right panel of Fig. 12).

The profile of horizontal velocity, u , at the front edge of the step is illustrated in Fig. 14. Results corresponding to four different time steps are highlighted in this figure. Note that, t^* , refers to the difference between the current time and the time at which water has reached the step. The horizontal velocity is seen to be negative near the step at the early stage of shipping. The velocity then increases and becomes positive ($t^* = 0.05$ s). With time, the gradient of the velocity becomes more significant, i.e., the magnitude of the negative values become larger compared to the previous time step as reported by Yan et al. (2018). Also, the speed value near the free surface (the height vertical position) becomes larger ($t^* = 0.1$ s). Later, the gradient of the horizontal velocity become less, while the horizontal velocity is still negative near the step ($t^* = 0.15$ s). Then, the velocity decreases strongly (see Skene et al., 2018), and negative values disappear ($t^* = 0.2$ s). Such a behaviour agrees with previous observations (Fig. 12), where it was seen that the energy flux reaches a peak value (which corresponds with large velocity observed at $t^* = 0.1$ s) and then highly decreases (which corresponds with large velocity observed at $t^* = 0.2$ s). The velocity profiles of different conditions are also compared. In the upper panel, velocity profiles of Cases 1 and 3 are compared (dam-break occurs in Tank 2). Case 3 has larger velocity gradient in comparison to Case 1 at the early stage of the shipping, which means that, when the freeboard becomes smaller, the flow is more turbulent, i.e., magnitude of negative and positive values of velocity profile become larger at the early stage ($t^* = 0.05$ s and $t^* = 0.1$ s).

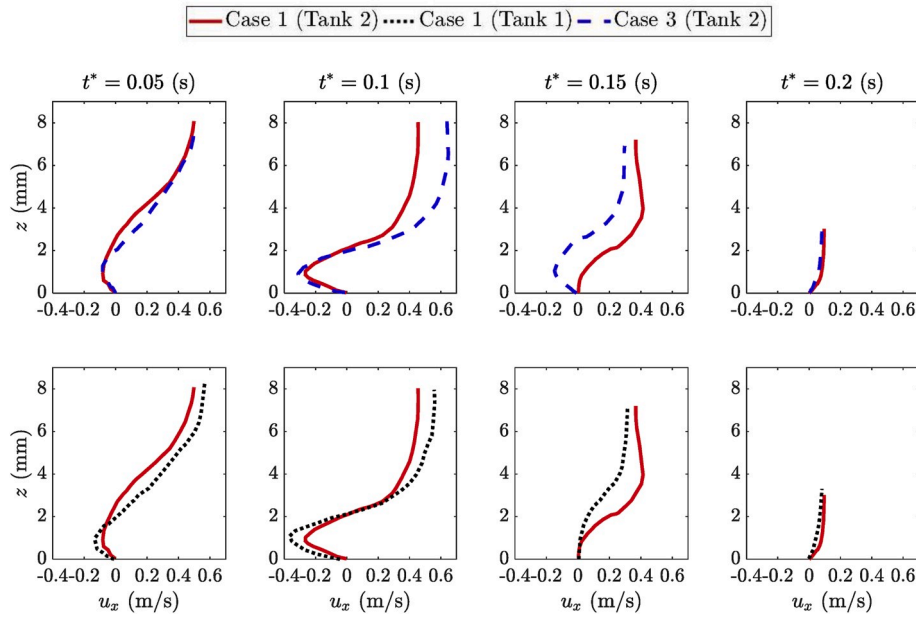


Fig. 14. Profile of the horizontal velocity of the shipping water at the front edge of the step at different times. The upper panels show a comparison between the velocity profiles of Cases 1 and 3 (Tank 2). The lower panels show the comparison between the velocity profiles for Case 1 in Tanks 1 and 2.

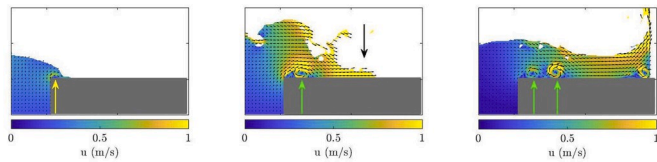


Fig. 15. Samples of the velocity plot of shipping water washing the step (grey box). The left panel shows the early stage of the washing as water reaches the step. The middle panel shows a point in time when the water has travelled some length over the step. The right panel shows a point in time at which water has reached the right wall of the tank. All simulations correspond to Case 5 and Tank 1.

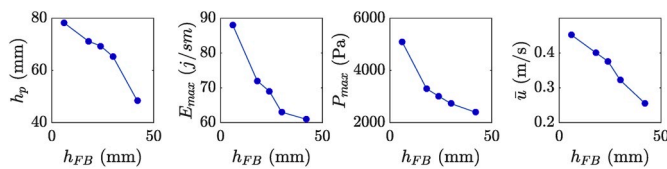


Fig. 16. Maximum values of (from left to right): water height (h_p), energy flux (E_{max}), hydrodynamic pressure (P_{max}) and mean horizontal velocity (\bar{u} , at time $t = 0.02$ s after water reaches the front edge of the step) as a function of freeboard (h_{FB}). (All results correspond to Tank 1).

However, the velocity of Case 1 becomes larger later. The lower panel of Fig. 14 shows comparisons between velocity profiles of Case 1 when the dam-break happens in Tanks 1 and 2. The velocity profile is observed to have larger gradient when the flow is running in Tank 1 (in which water travels less till it reaches the step) at the early stage of the washing. However, the velocity gradient of the shipping water occurring in Tank 2 becomes larger.

Fig. 15 shows the flow velocity direction and magnitude for Case 5 in Tank 1 at three times. The velocity magnitude is seen to be large near the edge of the step at the early stage (Fig. 15, left panel; the yellow arrow is pointing to the large value of the speed). The flow on the left side of the step is oriented upwards. At the next stage (Fig. 15, middle panel), the

water depth on the step has increased, and the edge of the bore (signalled by the black arrow in the figure) propagates at the highest speed. The vertical flow on the left side of the step presents a considerably lower speed compared to the front edge of the bore. A vortex appears on the step, near its front edge (green arrow). Finally, when the water has flowed over the entire step and reached the end wall of the tank (Fig. 15, right panel), it is driven upwards by the wall and large flow velocities occur. Compared to the previous stage, the flow velocity at the edge of the step is lower. There are three vortices now: one at the end of the step (at the angle with the wall), the previous one (which moved to the right) and a new one that appeared near the front edge (the two latter are indicated by green arrows in the figure). The velocity of the flow field on the left side of the step is lower than in the previous stages.

The summary of the results for the dam-break simulations in Tank 1 with $h_d/h_w = 0.6$ is illustrated in Fig. 16. The results presented in this figure include the peak value of water surface elevation (at a point with longitudinal position of $0.0130L_s$), maximum value of the energy flux, peak pressure and mean value of the horizontal velocity at an arbitrary point. The value of the mean velocity corresponds to 0.02 s after water reaches the front edge. The results presented show that the peak energy flux and the pressure increase as the freeboard decreases. Such a dependence (higher slope at smaller freeboard) is not observed for the surface elevation and velocity. Note that the velocity increases linearly with a decrease in freeboard, as reported by Song et al. (2015). The proportion of the kinematic energy has been computed for different cases (Fig. 17). The contribution of the kinematic energy of the fluid increases as the freeboard decreases, in line with the observations of Fig. 16.

4. Conclusions

Shipping water washing the upper surface of a fixed object was numerically modelled to improve our understanding of the physics of the flow (the velocity field, the vorticity, velocity profile and energy flux) as it impacts the deck and runs forward.

Numerical results were compared against the experimental data, and it was found that the turbulent simulations provide more accurate results of the shipping water phenomenon. When the laminar flow was considered, the free surface elevation and the impact force were over-

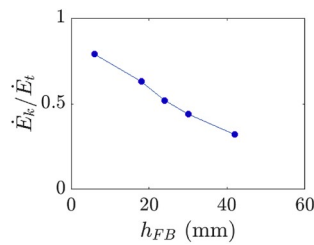


Fig. 17. Ratio of the kinematic energy flux (\dot{E}_k) to the total energy flux (\dot{E}_t) as a function of freeboard (h_{FB}). (All results correspond to Tank 1).

predicted both in the tank and over the step. It was shown that the maximum water height of the shipping flow washing the step increases as the freeboard decreases, which was associated with the energy flux. The energy flux of the water at the front edge of the step was observed to increase with a decrease in the freeboard. Moreover, the energy flux was found to be highly dependent on the mean velocity of the flow field as it reaches the edge of the step. For the cases with a small freeboard, the mean velocity was shown to be larger. Overall, it was shown that the role of kinematic energy in total energy flux becomes more significant as the freeboard becomes smaller. The energy flux of the tested cases in which the flow (caused by the dam-break) travels further to reach the step was found to be smaller, leading to smaller impact force and water height.

It was also observed that the energy flux of the solitary shipping water propagating over the step approaches negative values after a while, implying that water is driven back to the tank. The sampled velocity vectors showed that the horizontal velocity of the shipping water can become negative near the step, the extent of which is more significant for the cases with smaller freeboard. In such circumstances, a large velocity gradient occurs, and a moving-forward vortex appears. A further vortex, which is weaker compared to the previous one, was seen to emerge, following the previous vortex.

These conclusions can help ocean engineers to ensure safer conditions for the floating objects. In real sea conditions, ships and floating structures are subjected to ocean waves resulting in wave-induced vertical and flexural motions, which is the subject of the continuation of this work.

Declaration of competing interest

The authors declare that they have no known competing financial interests or personal relationships that could have appeared to influence the work reported in this paper.

CRediT authorship contribution statement

Danial Khojasteh: Conceptualization, Methodology, Writing - original draft, Writing - review & editing. **Sasan Tavakoli:** Software, Validation, Visualization, Writing - original draft. **Abbas Dashtimanesh:** Conceptualization, Writing - review & editing. **Azam Dolatshah:** Investigation, Writing - review & editing. **Luofeng Huang:** Software, Writing - review & editing. **William Glamore:** Conceptualization, Writing - review & editing. **Mahmood Sadat-Noori:** Writing - review & editing. **Gregorio Iglesias:** Conceptualization, Writing - review & editing.

Acknowledgements

Danial Khojasteh is funded by a UNSW Scientia PhD Scholarship. Sasan Tavakoli is supported by the Melbourne Research Scholarship provided by the University of Melbourne. Azam Dolatshah is supported by Swinburne University Postgraduate Research Award and Nortek AS.

References

- Amaro Jr RA, Cheng LY, Rosa SV, Numerical study on performance of perforated breakwater for green water, *J. Waterw. Port. Coast. Ocean Eng.*, 145(6): 04019021.
- Ariyaratne, K., Chang, K.A., Mercier, R., 2012. Green water impact pressure on a three-dimensional model structure. *Exp. Fluids* 53, 1879–1894.
- Bayoumi, S., Incecik, A., El-Gamal, H., 2015. Dynamic modelling of Spar-Buoy oscillating water column wave energy converter. *Ships Offshore Struct.* 108, 620–635.
- Buchner, B., 1995. On the impact of green water loading on ship and offshore unit design. In: *Proceedings of International Symposium of Practical Design of Ships and Mobile Units, PRADS'95*. The Society of Naval Architects of Korea, Seoul, pp. 430–443.
- Buchner, B., 2002. *Green Water on Ship-type Offshore Structures*. PhD Thesis. Delft TU, Delft, Netherlands.
- Chan, E.S., Melville, W.K., 1988. Deep-water plunging wave pressures on a vertical plane wall. *Phil. Trans. Math. Phys. Eng. Sci.* 417, 95–113.
- Chen, L., Taylor, P.H., Draper, S., Wolgamot, H., 2019. 3-D numerical modelling of greenwater loading on fixed ship-shaped FPSOs. *J. Fluid Struct.* 84, 283–301.
- Chuang, W.L., Chang, K.A., Mercier, R., 2015. Green water velocity due to breaking wave impingement on a tension leg platform. *Exp. Fluids* 56, 1–21.
- Cox, D.T., Scott, C.P., 2001. Exceedance probability for wave overtopping on a fixed deck. *Ocean Eng.* 28, 701–727.
- Cuomo, G., Allsop, W., Bruce, T., Pearson, J., 2010. Breaking wave loads at vertical seawalls and breakwaters. *Coast Eng.* 57, 424–439.
- Dashtimanesh, A., Ghadimi, P., 2013. A three-dimensional SPH model for detailed study of free surface deformation, just behind a rectangular planing hull. *J. Braz. Soc. Mech. Sci. Eng.* 35 (4), 369–380.
- Dashtimanesh, A., Tavakoli, S., Kohansal, A., Khosravani, R., Ghassemzadeh, A., 2020. Numerical study on a heeled one-stepped boat moving forward in planing regime. *Appl. Ocean Res.* 96, 102057.
- De Padova, D., Ben Meftah, M., De Seri, F., Mossa, M., Sibilla, S., 2019. Characteristics of breaking vorticity in spilling and plunging waves investigated numerically by SPH. *Environ. Fluid Mech.* <https://doi.org/10.1007/s10665>.
- Demirel, Y.K., Turan, O., Incecik, A., 2017. Predicting the effect of biofouling on ship resistance using CFD. *Appl. Ocean Res.* 62, 100–118.
- Dillingham, J.T., 1981. Motion studies of a vessel with water on deck. *Mar. Technol.* 18, 1.
- Dolatshah, A., Nelli, F., Alberello, A., Bennetts, L.G., Skene, D.M., Meylan, M.H., Monty, J.P., Toffoli, A., 2018. Waves through a continuous ice cover: ice breakup and wave attenuation. *Phys. Fluids* 20, 515.
- Ersdal, G., Kvitrud, A., 2000. Green water on Norwegian production ships. In: *Proceedings of the Tenth International Offshore and Polar Engineering Conference*.
- Esfandiari, A., Tavakoli, S., Dashtimanesh, A., 2019. Comparison between the dynamic behavior of the non-stepped and double-stepped planing hulls in rough water: a numerical study. *Journal of Ship Production and Design* 10, 5957/JSPD.11170053.
- Faltinsen, O.M., Greco, M., Landrini, M., 2002. Green water loading on a FPSO. *J. Offshore Mech. Arctic Eng.* 124, 97–103.
- Faltinsen, O.M., Greco, M., Landrini, M., 2004. Slamming in marine application. *J. Eng. Math.* 48, 448–475.
- Faltinsen, O.M., Zhu, X., Hu, C., 2005. Strongly nonlinear flows in seakeeping. Key note lecture. In: *Proceedings of ICRMT'05, Ischia, Italy*, p. 18.
- Fonseca and Soares CG, Experimental investigation of the shipping water on the bow of a containership, *J. Offshore Mech. Arctic Eng.*, 127, 322–330.
- Gatin, I., Vukcevic, V., Jasak, H., Seo, J., Rhee, S.H., 2018a. CFD verification and validation of green sea loads. *Ocean Eng.* 148, 500–515.
- Gatin, I., Cvijetic, G., Vukcevic, V., Jasak, H., Malenica, S., 2018b. Harmonic Balance method for nonlinear and viscous free surface flows 157, 164–179.
- Ghadimi, P., Farsi, M., Dashtimanesh, A., 2012. Study of various numerical aspects of 3D-SPH for simulation of the dam break problem. *J. Braz. Soc. Mech. Sci. Eng.* 34, 486–491.
- Ghadimi, P., Dashtimanesh, A., Farsi, M., Najafi, S., 2013. Investigation of free surface flow generated by a planing flat plate using smoothed particle hydrodynamics method and FLOW3D simulations, 227, 125–135.
- Ghadimi, P., Panahi, S., Tavakoli, S., 2019. Hydrodynamic study of a double-stepped planing craft through numerical simulations. *J. Braz. Soc. Mech. Sci. Eng.* 41, 1–15.
- Greco, M., Colicchio, Faltinsen O.M., 2007. Shipping of water on a two-dimensional structure. Part 2. *J. Fluid Mech.* 581, 371–399.
- Greco, M., Lugni, C., 2012a. 3-D seakeeping analysis with water on deck and slamming. Part 1: numerical solver. *J. Fluid Struct.* 33, 127–147.
- Greco, M., Lugni, C., 2012b. 3-D seakeeping analysis with water on deck and slamming. Part 2: experiments and physical investigation. *J. Fluid Struct.* 33, 148–179.
- Greco, M., Landrini, M., Faltinsen, O.M., 2001. Basic studies of water on deck. In: *Proceedings of Twenty-Third Symposium on Naval Hydrodynamics Office of Naval Research Basin d'Essais des Carenes*. National Research Council.
- Greco, M., Landrini, M., Faltinsen, O.M., 2004. Impact flows and loads on ship-deck structures. *J. Fluid Struct.* 19 (3), 251–275.
- Greco, M., Landrini, M., Faltinsen, O.M., 2005. Shipping of water on a two-dimensional structure. *J. Fluid Mech.* 525, 309–322.
- Greco, M., Lungu, C., Faltinsen, O.M., 2015. Influence of motion coupling and nonlinear effects on parametric roll for a floating production storage and offloading platform. *Phil. Trans. Math. Phys. Eng. Sci.* 373, 20140110.
- Gush, S., Reins, G., Koo, B., Wang, Z., yang, J., Stern, F., 2007. Plunging wave breaking: EFD and CFD. In: *Proceedings of International Conference on Violent Flows (VF-2007)*, Organized by RIAM. Kyushu University, Fukuoka, Japan.

- Hernández, I.D., Hernández-Fontes, J.V., Vitola, M.A., Silva, M.C., Espenranca, P.T.T., 2018. Water elevation measurements using binary image analysis for 2D hydrodynamic experiments. *Ocean. Eng.* 157, 325–338.
- Hernández-Fontes, J.V., Vitola, M.A., Silva, M.C., Espenranca, P.T.T., Sphaier, S.H., 2017. USE of wet dam-break to study green water problem. In: Proceedings of the ASME 2017 36th International Conference on Ocean, Offshore and Arctic Engineering, Trondheim, Norway.
- Hernández-Fontes, J.V., Vitola, M.A., Silva, M.C., Espenranca, P.T.T., Sphaier, S.H., 2018. On the generation of isolated green water events using wet dam-break. *J. Offshore Mech. Arctic Eng.* 140, 1–10.
- Hernández-Fontes, J.V., Vitola, M.A., Espenranca, P.T.T., Sphaier, S.H., 2019a. Analytical convolution model for shipping water evolution on a fixed structure. *Appl. Ocean Res.* 82, 415–429.
- Hernández-Fontes, J.V., Vitola, M.A., Espenranca, P.T.T., Sphaier, S.H., 2019b. Assessing shipping water vertical loads on a fixed structure by convolution model and wet dam-break tests. *Applied Ocean Engineering* 82, 63–73.
- Higuara, P., Lara, J.L., Losada, I.J., 2013. Simulating coastal engineering processes with openfoam. *Coast Eng.* 71, 119–134.
- Higuara, P., Lara, J.L., Losada, I.J., 2014a. Three-dimensional interaction of waves and porous coastal structures using openfoam. part I: formulation and validation. *Coast Eng.* 83, 243–258.
- Higuara, P., Lara, J.L., Losada, I.J., 2014b. Three-dimensional interaction of waves and porous coastal structures using openfoam. part II: Application. *Coast Eng.* 83, 259–270.
- Hirdaris, S.E., Bai, W., Dessi, D., Ergin, A., Gu, X., Hermundstad, O.A., et al., 2014. Loads for use in the design of ships and offshore structures. *Ocean. Eng.* 78, 131–171.
- Hirt, C., Nichols, B., 1981. Volume of fluid (vof) method for the dynamics of free boundaries. *J. Comput. Phys.* 39, 201–225.
- Huang, Z., Hsiung, C.C., 1996. Nonlinear shallow water on deck. *J. Ship Res.* 40, 1–13.
- Huang, L., Thomas, G., 2019. Simulation of wave interaction with a circular ice floe. *J. Offshore Mech. Arctic Eng.* 141, 041302.
- Huang, L., Ren, K., Li, M., Tukovic, Z., Cardiff, P., Thomas, G., 2019a. Fluid-structure interaction of a large ice sheet in waves. *Ocean. Eng.* 182, 102–111.
- Huang, L., Tuhkuri, J., Igrac, B., Li, M., Stagonas, D., Toffoli, A., Cardiff, P., Thomas, G., 2019b. Ship Resistance when Operating in Floating Ice Floes: a Combined CFD&DEM Approach, p. 10018 arXiv:1909.
- Huang, L., Li, M., Romu, T., Dolatshah, A., Thomas, G., 2020. Simulation of a ship operating in an open-water ice channel. *Ships Offshore Struct.* <https://doi.org/10.1080/17445302.2020.1729595>. Published Online.
- Hui, L., Haijiang, L., Liheng, C., Senxun, L., 2017. Experimental study on the dam-break hydrographs at the gate location. *J. Ocean Univ. China* 16, 679–702.
- Izadi, M., Ghadimi, P., Fadavi, M., Tavakoli, S., 2018a. Numerical modeling of the freefall of two-dimensional wedge bodies into water surface. *J. Braz. Soc. Mech. Sci. Eng.* 40, 1–24.
- Izadi, M., Ghadimi, P., Fadavi, M., Tavakoli, S., 2018b. Hydroelastic analysis of water impact of flexible asymmetric wedge with an oblique speed. *Meccanica* 53 (10), 2585–2617.
- Jalalisedi, M., Benbelkacem, G., Porfiri, M., 2018. Solid obstacles can reduce hydrodynamic loading during water entry. *Physical Review Fluids* 3, 074801.
- Jasak, H., 2009. OpenFOAM: open source CFD in research and industry. *Int. J. Nav. Archit. Ocean Eng.* 1, 89–94.
- Javanmardi, N., Ghadimi, P., Tavakoli, S., 2018. Probing into the effects of cavitation on hydrodynamic characteristics of surface piercing propellers through numerical modeling of oblique water entry of a thin wedge. *Brodogradnja: Teorija i praksa brodogradnje i pomorske tehnike* 69 (1), 151–168.
- Khojasteh, D., Kamali, R., 2016. Evaluation of wave energy absorption by heaving point absorbers at various hot spots in Iran seas. *Energy* 109, 629–640.
- Khojasteh, D., Kamali, R., 2017. Design and dynamic study of a ROV with application to oil and gas industries of Persian Gulf. *Ocean. Eng.* 136, 18–30.
- Khojasteh, D., Mousavi, S.M., Kamali, R., 2017. CFD analysis of Newtonian and non-Newtonian droplets impinging on heated hydrophilic and hydrophobic surfaces. *Indian J. Phys.* 91 (5), 513–520.
- Khojasteh, D., Mousavi, S.M., Glamore, W., Iglesias, G., 2018a. Wave energy status in Asia. *Ocean. Eng.* 169, 344–358.
- Khojasteh, D., Khojasteh, D., Kamali, R., Beyene, A., Iglesias, G., 2018b. Assessment of renewable energy resources in Iran; with a focus on wave and tidal energy. *Renew. Sustain. Energy Rev.* 81, 2992–3005.
- Kim, M., Hizir, O., Turan, O., Day, D., Incecik, A., 2017. Estimation of added resistance and ship speed loss in a seaway. *Ocean. Eng.* 141, 465–476.
- Kleefsman, K.M.T., Fekken, G., Veldman, A.E.P., Iwanowski, B., Buchner, B., 2005. A volume of fluid based simulation method for wave impact problems. *J. Comput. Phys.* 206, 363–393.
- Landrini, M., Colagrossi, A., Greco, M., Tulin, M.P., 2012. The fluid mechanics of splashing bow waves on ships: a hybrid BEM–SPH analysis. *Ocean. Eng.* 53, 111–127.
- Larsson, L., Stern, F., Visonneau, M., 2013. Numerical Ship Hydrodynamics: an Assessment of the Gothenburg 2010 Workshop. Springer Science & Business Media.
- Longuet Higgins, M.S., Cokelet, E.D., 1976. The deformation of steep surface waves on water: I A numerical method of computation. *Phil. Trans. Math. Phys. Eng. Sci.* 350, 1–26.
- Lopez, I., Pereira, B., Castro, F., Iglesias, G., 2014. Optimisation of turbine-induced damping for an OWC wave energy converter using a RANS–VOF numerical model. *Appl. Energy* 127, 105–114.
- Masida, M., Sasahara, Y., Minami, K., Tezdogan, T., Incecik, A., 2019. Use of the Mps method to estimate the energy conversion efficiency of the owc-wec (first report). *Ocean. Eng.* 106133.
- Mori, N., Cox, D.T., 2003. Dynamic properties of green water event in the overtopping of extreme waves on a fixed dock. *Ocean. Eng.* 30, 2021–2052.
- Na, B., Chang, K.A., Huang, Z.C., Lim, H.J., 2016. Turbulent flow field and air entrainment in laboratory plunging breaking waves. *J. Geophys. Res.: Oceans* 121, 2980–3009.
- Nakagawa, H., Nakamura, S., Ichihashi, K., 1969. Generation and Development of a Hydraulic Bore Due to the Breaking of a Dam. Bulletin of the Disaster Prevention Research Institute, Kyoto University, Kyoto, Japan.
- Niazmand Biland, R., Dashtimanesh, A., Tavakoli, S., 2020. Hydrodynamic study of heeled double-stepped planing hulls using CFD and 2D+ T method. *Ocean. Eng.* 196, 106813.
- Nielsen, K.B., Mayer, S., 2004. Numerical prediction of green water incidents. *Ocean. Eng.* 31, 363–399.
- Ogawa, Y., Miami, M., Tanziawa, K., Kumano, A., Matsunami, R., Hayashi, T., et al., 2002. Shipping water load due to deck wetness. In: Proceedings of the Twelfth International Offshore and Polar Engineering Conference (ISOPE). Kitakyushu, Japan.
- O’Dea, J., Powers, E., Zselecsky, J., 1992. Experimental determination of non-linearities in vertical plane ship motions. In: Proceedings of 19th Symposium on Naval Hydrodynamics, Seoul, Korea, pp. 73–91.
- Ryu, Y., Change, K.-A., Mercier, R., 2007. Application of dam-break flow to green water prediction. *Appl. Ocean Res.* 29 (3), 128–136.
- Schonberg, T., Rainey, R.C.T., 2002. A hydrodynamic model of green water incidents. *Appl. Ocean Res.* 24, 299–307.
- Silva DFC, Esperanca PTT, Couthinho ALGA, Green water loads on FPSOs exposed to beam and quartering seas, Part II: CFD simulations, *Ocean. Eng.*, 140, 434–452.
- Skene, D.M., Bennetts, L.G., Wright, M., Meylan, M.H., Maki, K.J., 2018. Water wave overwash of a step 839, 293–312.
- Song, Y.K., Chang, K.A., Ariyaratne, K., Mercier, R., 2015. Surface velocity and impact pressure of green water flow on a fixed model structure in a large wave basin. *Ocean. Eng.* 104, 40–51.
- Stansby, P.K., Chegini, A., Barnes, T.C.D., 1998. The initial stages of a dam-break flow. *J. Fluid Mech.* 374, 407–424.
- Stern, F., Wilson, R.V., Coleman, H.W., Paterson, E.G., 2001. Comprehensive approach to verification and validation of CFD simulations—part I: methodology and procedures. *J. Fluid Eng.* 123, 793–802.
- Stern, F., Wilson, R., Shao, J., 2006. Quantitative V&V of CFD simulations and certification of CFD codes. *Int. J. Numer. Methods Fluid.* 50 (11), 1335–1355.
- Taha, T., Lateef, A.O.A., Pu, J.H., 2018. Laminar and turbulent analytical dam break wave modelling on dry-downstream open channel flow. *Fluid Mechanics Research International Journal* 2, 177–180.
- Tavakoli, S., Dashtimanesh, A., 2019. A six-DOF theoretical model for steady turning maneuver of a planing hull. *Ocean. Eng.* 189, 106328.
- Tezdogan, T., Demirel, Y.K., Kellett, P., Khorasanchi, M., Incecik, A., Turan, O., 2015. Full-scale unsteady RANS CFD simulations of ship behaviour and performance in head seas due to slow steaming. *Ocean. Eng.* 97, 186–206.
- Vukcevic, V., Gatin, I., Jasak, H., 2018. The naval hydro pack: current status and challenges. In: Proceedings of 13th OpenFOAM Workshop.
- Whitham, G.B., 1962. Mass, momentum and energy flux in water waves. *J. Fluid Mech.* 12 (1), 135–147.
- Xie N, Hann M, Pemberton R, Iglesias G, Greavers D, A numerical and experimental investigation of the effect of side walls on hydrodynamic model testing in a wave flume, *Ocean. Eng.*, 186, 106108.
- Yan, B., Bai, W., Qian, L., Ma, Z., 2018. Study on hydro-kinematic characteristics of green water over different fixed decks using immersed boundary method. *Ocean. Eng.* 164, 74–86.
- Yilmaz, O., Incecik, A., Han, J.C., 2003. Simulation of green water flow on deck using non-linear dam-breaking theory. *Ocean. Eng.* 30, 601–610.
- Yilmaz, O., Korobkin, A., Iafirati, A., 2013. The initial stage of dam-break flow of two immiscible fluids. Linear analysis of global flow, *Applied Ocean Research* 42, 60–69.
- Zech, Y., Soares-Fraza, S., 2007. Dam-break flow experiments and real-case data. A database from the European IMPACT research. *J. Hydraul. Res.* 45, 5–7.
- Zhang, X., Draper, S., Wolgamot, Zhao, W., Cheng, L., 2019. Eliciting features of 2D greenwater overtopping of a fixed box using modified dam break models. *Appl. Ocean Res.* 84, 74–91.
- Zhou, D., Chan, E.S., Melville, W.K., 1991. Wave impact pressure on vertical cylinders. *Appl. Ocean Res.* 13, 220–234.
- Zhou, Y., Xiao, Q., Liu, Y., Incecik, A., Peyrard, C., Li, S., Pan, G., 2019. Numerical modelling of dynamic responses of a floating offshore wind turbine subject to focused waves. *Energies* 12, 3482.